Catalytic dehydrogenation of ethanol over zinc-containing zeolites

Gao, Kai; Mielby, Jerrik; Kegnæs, Søren

Published in:
Catalysis Today

Link to article, DOI:
10.1016/j.cattod.2022.06.023

Publication date:
2022

Document Version
Publisher's PDF, also known as Version of record

Catalysis Today 405-406 (2022) 144–151

Contents lists available at ScienceDirect

Catalysis Today

journal homepage: www.elsevier.com/locate/cattod

Catalytic dehydrogenation of ethanol over zinc-containing zeolites

Kai Gao, Jerrik Mielby, Søren Kegnæs *

DTU Chemistry, Technical University of Denmark, Kemitorvet 207, DK-2800 Kgs. Lyngby, Denmark

ARTICLE INFO

Keywords:
Ethanol
Acetaldehyde
Dehydrogenation
Zinc
MFI zeolite

ABSTRACT

Catalytic dehydrogenation of ethanol produces acetaldehyde, an important precursor for several value-added chemicals such as acetic acid and acetate esters. In this paper, we demonstrate that Zn-containing MFI zeolites are highly active and selective catalysts for this process. Furthermore, we show that their activity and selectivity depend on the chemical composition and preparation of the catalysts. The best catalyst comprises 5 wt % Zn on Silicalite-1 zeolite and results in 65.2% conversion and 94.5% selectivity towards acetaldehyde at 400 ℃. We relate the high selectivity to the absence of Brønsted acidic silanol groups, which suppresses the dehydration of ethanol into ethylene. Furthermore, while pure HZSM-5 and NaZSM-5 zeolites result in dehydration products, such as ethylene and diethyl ether, Zn on NaZSM-5 zeolite also results in acetaldehyde, which confirms that Zn is the active site. Finally, we compare different preparation procedures to show that several Zn-species may be active for the catalytic reaction.

1. Introduction

Acetaldehyde (CH_3CHO) is an important precursor for the industrial production of acetic acid, ethyl acetate, and pyridine. It is typically produced via the Wacker process, which oxidizes ethylene to acetaldehyde under acidic aqueous conditions and in the presence of a $PdCl_2$ and $CuCl_2$ catalyst [1,2].

Alternatively, acetaldehyde may be produced from the dehydrogenation of bioethanol, a renewable feedstock made by fermentation of waste biomass [3]. In general, there are two methods to produce acetaldehyde from ethanol, via selective oxidation or dehydrogenation [4–8]. While selective oxidation requires an oxidant, selective dehydrogenation results in the formation of dihydrogen, which may be used for further chemical or energy conversion.

Over time researchers have investigated a large number of catalysts for the ethanol conversion into acetaldehyde, and specifically copper [9–15], magnesium [16], nickel [17–20], zinc [14,21–24], and gold [20,25–28] has attracted much interest. Cu-based catalysts were surveyed extensively due to their high catalytic activity and selectivity for acetaldehyde production [13–15]. Unfortunately, Cu-based catalysts often suffer from rapid deactivation caused by sintering, which remains a significant challenge due to the relatively low melting point of metal Cu [29,30]. Stephanopoulos and co-workers showed that adding a trace amount of Ni effectively limited the sintering [18] and Busca and co-workers discovered that Cu nanoparticles formed on the Zn-poor areas of the $ZnAl_2O_4$ support increased the thermal stability [11]. Au-based catalysts are also promising for ethanol dehydrogenation due to the weak binding of adsorbed ethoxy species. Interestingly, the highest catalytic activity is observed at a particular nanoparticle size of 6 nm, which may be related to the particle geometry and the facile cleavage of the β-H atom in the absorbed ethoxide on the Au surface [26]. However, the high cost of Au limits its industrial applications and urges the exploration of other non-noble metal substitutes like Zn.

Park and co-workers studied the mechanism of ethanol dehydrogenation to acetaldehyde using Zn catalysts using an isotope tracing method. The authors proposed that the reaction involves a hydride transfer. In the proposed mechanism, the O atom and the β-H atoms are attached to adjacent Zn atoms when ethanol absorbs on the ZnO surface. The adsorbed ethanol then forms an ethoxy species. The electron-deficient Zn receives an electron from β-C, thus leading to the formation of $\beta\text{-}C^{\delta+}$ with a positive charge. Meanwhile, the β-H is easily abstracted by the Zn atom to form a Zn–H bond. Subsequently, the α-H shifts to $\beta\text{-}C^{\delta+}$ with an electron pair that results in Zn–O bond cleavage and the formation of the C═O group in acetaldehyde [23].

Ouyang and co-workers studied the pure ZnO catalyst for ethanol dehydrogenation and found that it does not show any activity at temperatures below 165 ℃ [31]. Therefore, other researchers has also investigated other supported and composite Zn-based catalysts. For instance, Miyake and co-workers investigated the ZnO/SiO_2 catalyst and found it exhibited moderate ethanol conversion but excellent stability

* Corresponding author.
E-mail address: skk@kemi.dtu.dk (S. Kegnæs).

https://doi.org/10.1016/j.cattod.2022.06.023
Received 21 January 2022; Received in revised form 30 May 2022; Accepted 27 June 2022
Available online 28 June 2022

and selectivity of acetaldehyde. The rate-determination step for ZnO/-SiO_2 catalyst was confirmed to be the simultaneous dissociation of O–H and α–H bonds [14]. Taylor and co-workers proposed that ZnO impregnated on mordenite (MOR) support can suppress the carbonaceous deposition in the ethanol conversion to acetaldehyde [24]. Another function of ZnO was passivating the strong Lewis acidic sites in ZrO_2 to form $ZnZrO_x$ nanoparticle composites moderate acid-base balance [28,32]. These studies indicate that zeolites are promising support for Zn due to their high thermal stability and chemical resistance in the ethanol dehydrogenation to acetaldehyde process.

Here, we investigate different zinc-containing zeolites materials such as Zn/ZSM-5, Zn/Silicalite-1, and Zn-MFI catalytic performance in ethanol conversion to acetaldehyde. The Zn/ZSM-5 and Zn/Silicalite-1 zeolites were prepared by the incipient wetness impregnation, while the Zn-MFI catalyst was prepared through direct incorporation of Zn into the zeolite framework during the hydrothermal synthesis. The synthesized materials were characterized using XRD, N_2-physisorption, XPS, SEM, XRF, NH_3-TPD and tested in the ethanol dehydrogenation process. The results show that high catalytic activity relates to the absence of Brønsted acidic sites and that several Zn-species may be active for the catalytic reaction.

2. Experimental

2.1. Materials

Tetrapropylammonium hydroxide solution (TPAOH, 1.0 M in H_2O), tetraethyl orthosilicate (TEOS, ≥99.0%), sodium aluminate ($NaAlO_2$), Zn powder, ZnO powder, zinc nitrate hexahydrate ($Zn(NO_3)_2.6H_2O$, 98%), LUDOX® AS-40 colloidal silica (40 wt% suspension in H_2O), ethylene (≥99.5%) and acetaldehyde (≥99.5%) were received from Sigma-Aldrich and used without further purifications. Ethanol (≥99.6%) was obtained from VWR. NH_4-ZSM-5 (CBV 28014, molar ratio of $SiO_2/Al_2O_3 = 280$) was provided from Zeolyst.

2.2. Synthesis of catalysts

In this study, we synthesized four types of Zn-containing zeolites. For comparison, we also prepared pure zeolites without zinc. Silicalite-1 zeolite was synthesized according to our previously reported procedures [33,34], and Zn/Silicalite-1 was prepared by conventional incipient wetness impregnation.

In brief, 4.47 ml TEOS was added dropwise into 7.24 ml TPAOH solution under stirring in a Teflon beaker. The gel was then transferred into a stainless-steel autoclave and heated at 180 °C. After 72 h, the autoclave was quenched in water. The solid product was collected by vacuum filtration and washed thoroughly with deionized water until neutral pH. The zeolite was dried at 80 °C overnight and then calcined at 550 °C for 20 h with 4 h heating ramp. The synthesized zeolite was denoted as Silicalite-1 zeolite.

The Zn/Silicalite-1 was prepared by conventional incipient wetness impregnation using the as-prepared zeolite as Supporting material. First, the Silicalite-1 (1.0 g) was dried in a vacuum oven overnight. Then the desired amount of $Zn(NO_3)_2.6H_2O$ was dissolved into a small amount of water (equal to the total pore volume as determined by N_2-physisorption analysis) and impregnated dropwise on the zeolite under vigorous stirring. The impregnated zeolite was dried overnight and then calcined at 550 °C for 4 h with a 2-h heating ramp to decompose the $Zn(NO_3)_2$.

The NaZSM-5 zeolite was synthesized as the same method for the synthesis of Silicalite-1 zeolite except for the addition of 0.0164 g $NaAlO_2$ to 7.24 ml TPAOH solution under stirring before 4.47 ml TEOS addition. The molar ratio of SiO_2/Al_2O_3 of the prepared NaZSM-5 zeolite was 280. Meanwhile, the commercial zeolite NH_4-ZSM-5 was calcined at 550 ℃ for 2 h to obtain H-ZSM-5 before further use.

The Zn/NaZSM-5 and Zn/HZSM-5 catalysts were prepared by the same method as the aforementioned Zn/Silicalite-1 synthesis.

A Zn-MFI zeolite was prepared according to a method disclosed by British Petroleum (BP).[35] In brief, 2.0 g $Zn(NO_3)_2.6H_2O$ was dissolved in 5.0 g deionized water followed by dropwise addition of an aqueous ammonia solution. The obtained precipitate was washed with deionized water and then added an aqueous solution of 0.85 g NaOH and 18.0 g H_2O. 10.5 ml TPAOH and 15.02 g Ludox AS40 were added to the aforementioned solution to form a gel. The prepared gel was sealed in an autoclave and heated to 175 ℃ for 4 days. The product was collected by Buchner filtration, washed with water, dried, and then calcined at 550 ℃ for 18 h.

2.3. Characterization methods

X-ray powder diffraction patterns were recorded in transmission mode using Cu -Kα radiation from a focusing quartz monochromator and a Huber G760 Guinier camera in the 2θ interval 5–55°.

Nitrogen physisorption analysis were performed at liquid nitrogen temperature (77 K) on a Micromeritics 3 FLEX instrument. The samples were outgassed under a vacuum at 400 °C before measurement. The total surface area was calculated according to the BET method. The meso- and micropore volumes were determined by the BJH method (desorption branch) and the *t*-plot method, respectively.

X-ray photoelectron spectroscopy (XPS) was performed on a Thermo Fischer Scientific K-Alpha™ with a monochromated Al Kα X-ray source. The analysis was performed at pressures around 2×10^{-9} mbar. The spectra were recorded with 0.1 eV steps and with a pass energy of 50 eV and a spot size of 400 mm. 50 scans were performed for elemental analysis.

Scanning electron microscopy (SEM) was performed on Quanta 200 ESEM FEG operated at 10 kV, with the calcined zeolite samples placed on a carbon film. Before the analysis, the samples were coated with gold for five seconds.

X-ray fluorescence spectroscopy (XRF) measurements were performed with a PANalytical Epsilon-3XL instrument. The glass disc was made through the mixing of sample and flux by fusion at the temperature of 1050 ℃. The Zn loading was calculated through the calibration line.

Ammonia temperature-programmed desorption (NH_3-TPD) was conducted on a Micromeritics AutoChem II equipped with a thermal conductivity detector (TCD) calibrated for ammonia. The samples were heated to 500 °C before the adsorption of NH_3. The excess physically adsorbed NH_3 was removed by the inert gas flow, and desorption of NH_3 was carried out by increasing the temperature to 500 °C.

2.4. Catalytic tests

The catalytic performance tests were performed in a 4 mm inner-diameter quartz fix-bed reactor using 150 mg of fractionated catalyst 150–355 μm) fixed by two pieces of quartz wool. The reaction temperature was controlled by a thermocouple positioned inside the middle of the reactor. In a typical run, EtOH was fed by an HPLC pump with a flow of 0.05 ml/min. A nitrogen flow of 50 ml/min was used as carrier gas. The quantification of products was analyzed by an online GC with a flame ionization detector (FID) and a DB-1 non-polar capillary column. All products were identified by the retention time of standard compounds and confirmed by GC-MS. The ethanol conversion and product selectivity were calculated based on carbon balance as determined from the GC peak area. Each conversion and selectivity were the average value of three consecutive sample injections at the same temperature. The catalyst stability test was conducted at the desired temperature for 68 h and then regenerated by the calcination within the air at 550 ℃ for 24 h.

3. Results and discussions

3.1. Catalyst characterization

The physisorption isotherms in Fig. 1 show typical type I (top right) and type IV (top left, bottom left, and right) isotherms. While Zn/NaZSM-5 mainly contains micropores, the significant hysteresis loops in the Zn/HZSM-5 isotherms also reveal a mesoporous structure. According to previous literature, we ascribe the small hysteresis loop at $p/p^0 = 0.17$ in the Zn/HZSM-5 zeolite isotherms to a fluid-to-crystal-like phase transition typically observed in MFI zeolites [33]. The texture properties of Zn-containing zeolites are provided in Table S1, which confirms the mesoporous structure of Zn/HZSM-5 zeolite from the comparison between the surface area of total pores and micropores.

The XRD patterns of the Zn-impregnated and -incorporated zeolites are shown in Fig. 2. As expected, the four XRD patterns are consistent with the MFI structure with characteristic peaks at 2θ values of 7.8°, 8.9°, 23.1°, and 23.9°.[25,36] The impregnation of zinc species has little effect on the MFI zeolites. In general, we only observed a small peak from bulk ZnO at $2\theta = 36.3°$ in the Zn/Silicalite-1, 5%Zn/HZSM-5, and 5%Zn/NaZSM-5 samples (JCPDS Card No. 65-3411). We speculate that this peak may originate from relatively small is evidence of ZnO particles present in the mesopores or surface of Silicalite-1, HZSM-5, and NaZSM-5. In general, the relatively weak signal from ZnO indicates high Zn species dispersion. Furthermore, the Zn loading of four zeolites was confirmed by XRF measurement as shown in Table S2.

Fig. 3 shows the XPS analysis of the Zn modified zeolites at the Zn2p level. In general, the intensity of Zn-MFI is significantly lower than the Zn impregnated catalysts. We speculate that this observation may be explained by the successful incorporation of Zn in the MFI framework and the low amount of Zn on the external. The fitting curve of Zn XPS spectra around 1045.5 eV and a satellite peak at 1049.2 eV (only exist in 5%Zn/HZSM-5) belongs to Zn $2p_{1/2}$. Meanwhile, the two fitting peaks of Zn $2p_{3/2}$ spectra with the binding energy at 1022.6 eV and 1025.8 eV are assigned to ZnO (Zn-O bond) and $[ZnOZn]^{2+}$ species, separately [37,38]. The presence of $[ZnOZn]^{2+}$ species in the 5%Zn/HZSM-5 may occur from the dehydration of two $[ZnOH]^{+}$ species, while the $[ZnOH]^{+}$ species can result from protonation of ZnO [37]. The fitting peaks with binding energy at 1021.1 eV (5%Zn/Silicalite-1) and 1021.3 eV (5% Zn/NaZSM-5) are assigned to the ZnO cluster, which disperses on the surface of catalysts. Furthermore, the Zn $2p_{1/2}$ binding energy peaks at the binding energy of 1044.1 eV (Zn/Silicalite-1 and Zn/NaZSM-5) suggesting the presence of $[ZnOH]^{+}$ species [39].

The SEM morphologies of the various MFI-type zeolites are shown in Fig. 4. The SEM analysis shows that the prepared zeolites appear to be high crystallization through SEM images (Fig. 4). The well-defined terraces Zn-MFI zeolite appeared as polycrystalline spherical morphology with a hierarchical structure, which was different from Zn/Silicalite-1, Zn/HZSM-5, and Zn/NaZSM-5 zeolites. The hierarchical flakes of Zn-MFI demonstrate the Zn component in the zeolite synthesis system

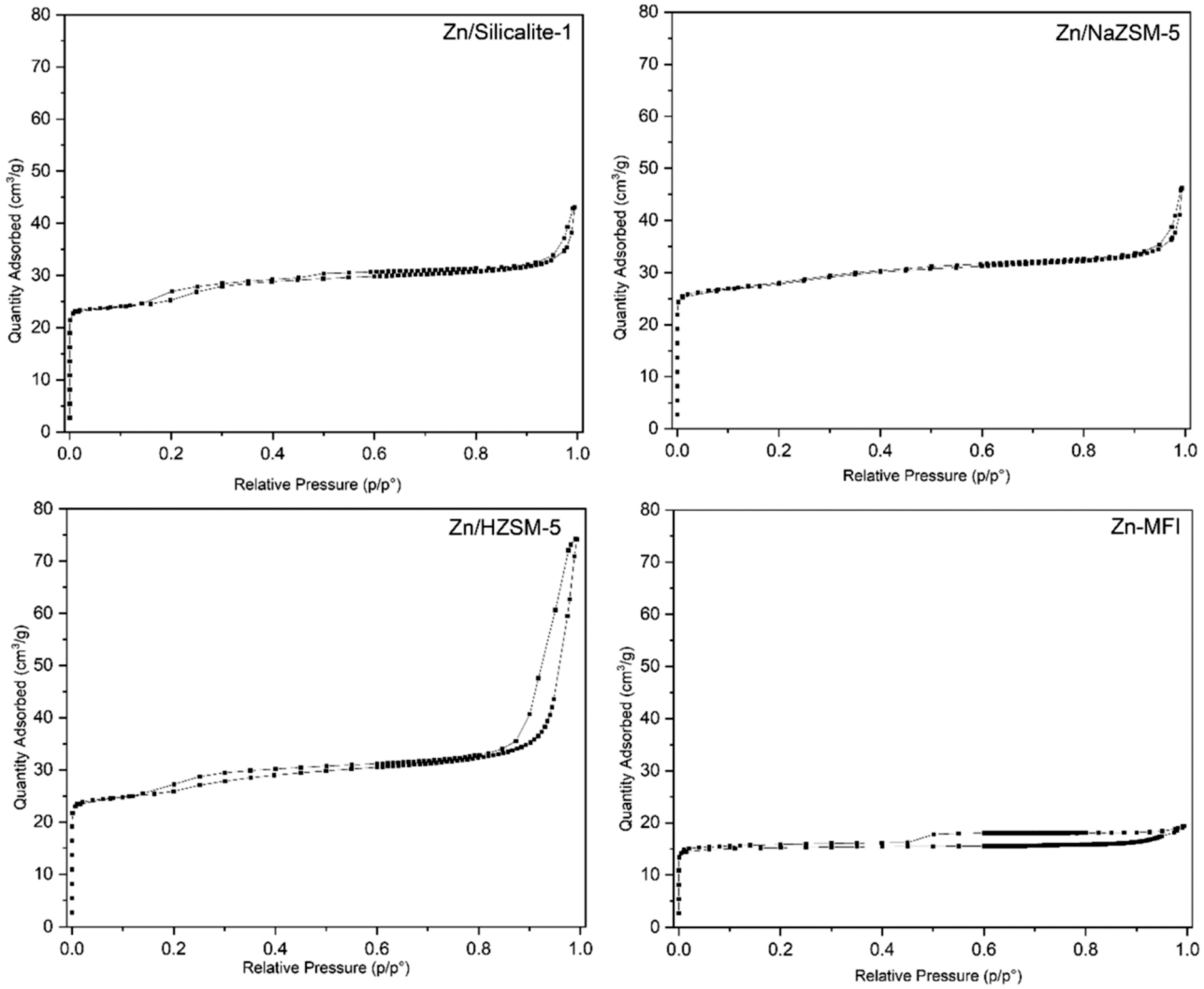

Fig. 1. N_2 physisorption analysis of Zn/Silicalite-1 (top left), Zn/NaZSM-5 (top right), Zn/HZSM-5 (bottom left), Zn-MFI (bottom right).

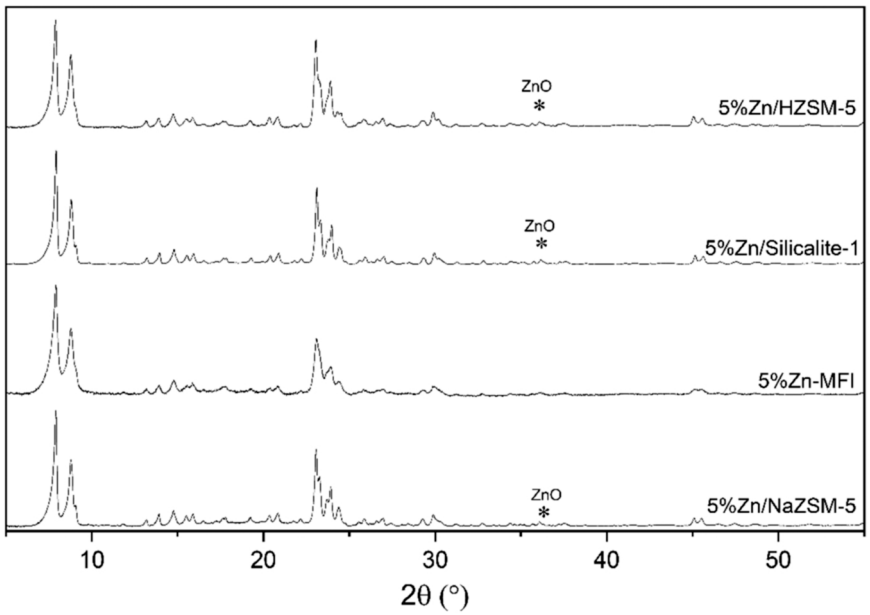

Fig. 2. XRD patterns for the prepared Zn contained zeolites.

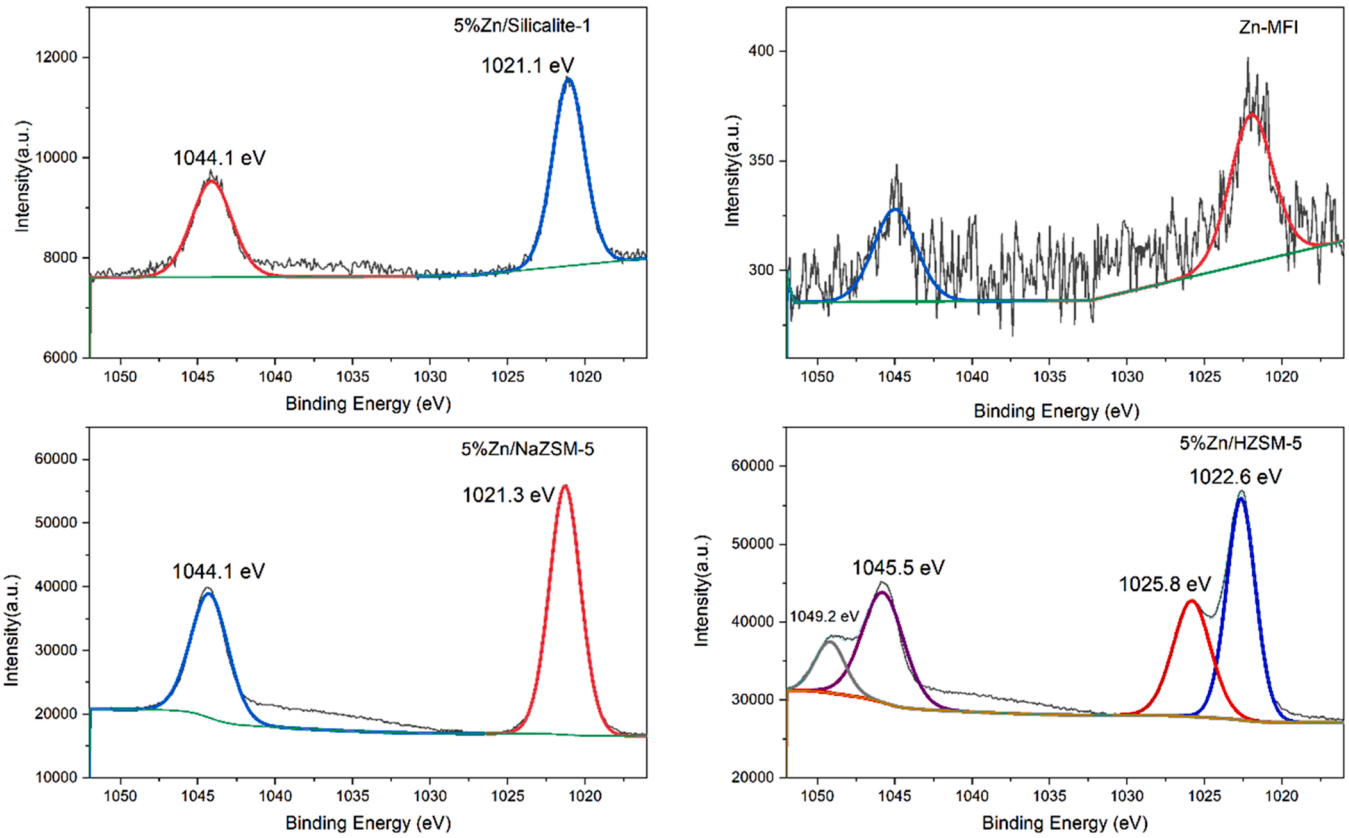

Fig. 3. XPS spectra of prepared Zn-containing zeolites at Zn2p level.

affects the crystal growth process, which is in favor of the formation of the nanocrystals [39]. The coffin-shaped Zn/Silicalite-1, Zn/HZSM-5, and Zn/and ZSM-5 zeolites were likely cuboid morphology, which is a typical shape for MFI synthesized using TPAOH as the structure-directing agent [34,40]. The Zn element mapping exhibits the uniform distribution of Zn in the Zn-containing zeolites as shown in Fig. S1.

3.2. *Catalytic performance*

Fig. 5 shows the conversion and selectivity for the catalytic dehydrogenation of ethanol over pure ZnO and 5%Zn/Silicalite-1. While pure Zn is completely inactive even at high temperatures (Fig. S2 left), pure ZnO results in some catalytic conversion and selectivity towards acetaldehyde and ethylene. Compared to pure ZnO, the zeolite-supported

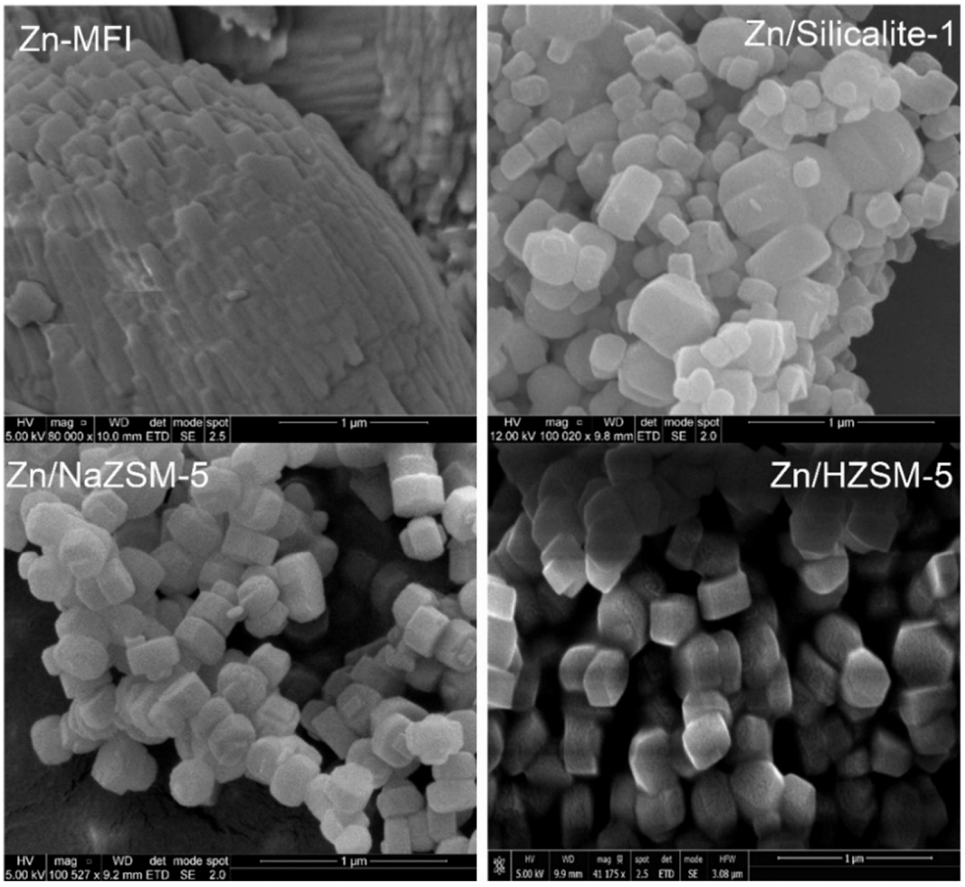

Fig. 4. SEM images of synthesized Zn-containing zeolite catalysts.

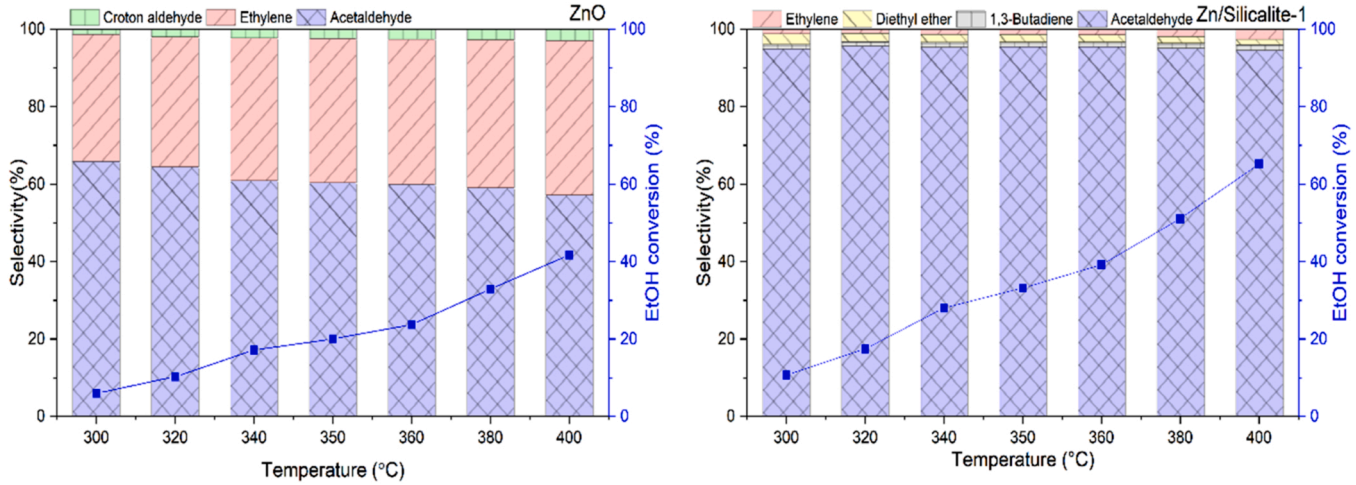

Fig. 5. Conversion and selectivity for the catalytic dehydrogenation of ethanol over pure ZnO (left) and Zn/Silicalite-1 (right) catalysts.

ZnO catalysts resulted in a significantly higher selectivity towards acetaldehyde. While pure Silicalite-1 had very little catalytic activity and mainly resulted in small amounts of ethylene (Fig. S2 right), 5%Zn/Silicalite-1 resulted in a conversion of 11–65% and a selectivity of > 95% between 300 and 400 °C. In general, the selectivity slightly decreased above 360 ℃, although the competing selectivity towards ethylene stayed below at all temperatures. Compared to the poor catalytic properties of pure Silicalite-1, these data confirmed that the Zn was responsible for the high catalytic activity. Furthermore, we noted that weakly acidic silanol groups in Silicalite-1 may be responsible for the dehydration of ethanol, which results in the formation of the main by-products ethylene and diethyl ether. In general, we observed more diethyl ether at lower temperatures and more ethylene at higher temperatures. The equilibrium between intermolecular and intramolecular dehydration at different temperatures was also in good agreement with the previous thermodynamic calculations [11]. Stability test and regeneration of Zn/Silicalite-1 zeolite catalyst were also performed at 400 ℃ as shown in Fig. S3, and it indicates the superior catalytic stability and regeneration activity in the continuous reaction of 68 h.

To investigate the catalytic effect of the Al in the framework, which is

different from the aforementioned Silicalite-1 zeolite, we also prepared a series of Zn-containing catalysts supported on the highly acidic MFI zeolite HZSM-5. Fig. 6 (left) and Fig. S4 (left) show the catalytic conversion and selectivity of 5% Zn/HZSM-5 and HZSM-5, respectively. As expected, the catalysts resulted in high conversions of ethanol, but a complete change in selectivity towards the dehydration products, particularly ethylene. Ethylene was the main product for both pure HZSM-5 and Zn/HZSM-5 catalysts, even with increasing loadings of Zn from 1 wt% to 5 wt% (Fig. S4 right and Fig. 6 left). These results may be explained by the high acidity of ZSM-5 on proton form (Table. S3), which easily facilitates the acid-catalyzed dehydration of ethanol into ethylene. Compared to pure HZSM-5, the 5%Zn/HZSM-5 catalysts did result in slightly lower conversion and slightly higher selectivity towards acetaldehyde. We speculate that this observation may be explained by the formation of $[ZnOH]^+$ species, which decreases the acidity and have some catalytic activity for dehydrogenation. The formation of $[ZnOH]^+$ is consistent with the higher binding energy peak observed by the XPS analysis in Fig. 3. For the Na-form of ZSM-5, however, ZnO was the main Zn component and it has an entirely different products distribution compared to the proton-form of ZSM-5. For comparison, pure NaZSM-5 only resulted in a limited conversion of ethanol and primarily dehydration products, including both diethyl ether and ethylene (Fig. S5). Over 5%Zn/NaZSM-5, the conversion increased and the product selectivity shifted towards acetaldehyde. This confirmed that ZnO particle on Na-ZSM-5 zeolite plays a critical role in the catalytic cycle. Compared to 5%Zn/Silicalite-1, we observed a slightly lower selectivity due to an increased formation of 1,3-butadiene. Interestingly, this indicates that the Zn-loaded and Na-exchanged zeolite has multiple active sites that can catalyze the transformation of ethanol into 1,3-butadiene. This process is believed to involve several consecutive steps, including 1) the dehydrogenation of ethanol into acetaldehyde, 2) an aldol condensation into acetaldol, 3) a dehydration into crotonaldehyde, 4) an Meerwein-Ponndorf-Verley (MPV) reaction into crotyl alcohol, and 5) a dehydration into 1,3-butadiene (Fig. 7).

To further investigate the catalytic effect of the nature of active Zn sites, we also prepared a Zn-based zeolite, where the Zn was incorporated in the MFI framework during the hydrothermal synthesis as previously disclosed by BP [35]. Although the as-prepared Zn-MFI catalyst only resulted in < 15% conversion, the selectivity towards acetaldehyde was almost 100%. Only at 400 °C, we started to observe small amounts of ethylene. Compared to 5%Zn/Silicalite-1, the 5%Zn-MFI catalyst resulted in a significantly lower conversion, indicating that the framework Zn has a lower catalytic activity than supported ZnO. In contrast, the high selectivity indicates that the direct incorporation of Zn may result in fewer acidic silanol groups that cause the formation of dehydration products.

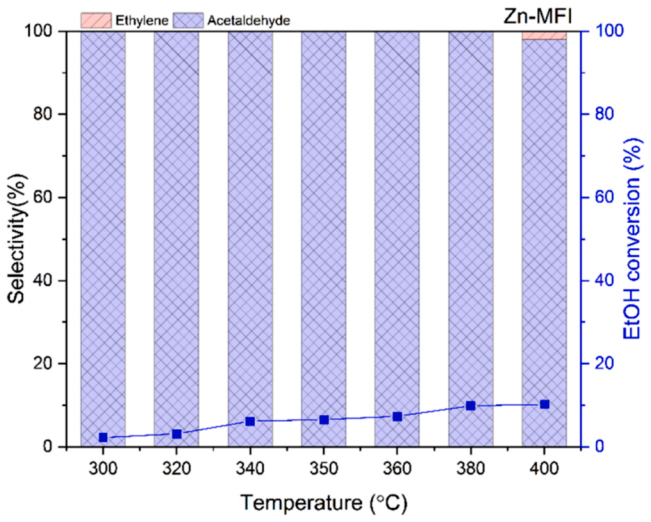

Fig. 7. The conversion and selectivity for the catalytic dehydrogenation of ethanol over 5%Zn-MFI catalyst.

4. Conclusions

In conclusion, we have demonstrated that ZnO supported on Silicalite-1 and NaZSM-5 are effective catalysts for ethanol dehydration at temperatures between 300 and 400 °C. In contrast, ZnO supported on the acidic HZSM-5 on proton form catalyzes the dehydration of ethanol, which results in the formation of ethylene. This reaction is not only catalyzed by the strongly acidic Al sites, but also by the less acidic silanol groups. Therefore, the 5% Zn/Silicalite-1 resulted in the highest productivity, reaching 65% conversion and 95% selectivity at 400 °C. Finally, we compared the catalytic performances of pure NaZSM-5, Zn/HZSM-5, and Zn/NaZSM-5 zeolites, which demonstrated entirely different reaction processes of dehydration and dehydrogenation, respectively. The different preparation procedures of Zn-containing zeolites show that several Zn-species may be active for the catalytic reaction, although ZnO appears to be the most active component.

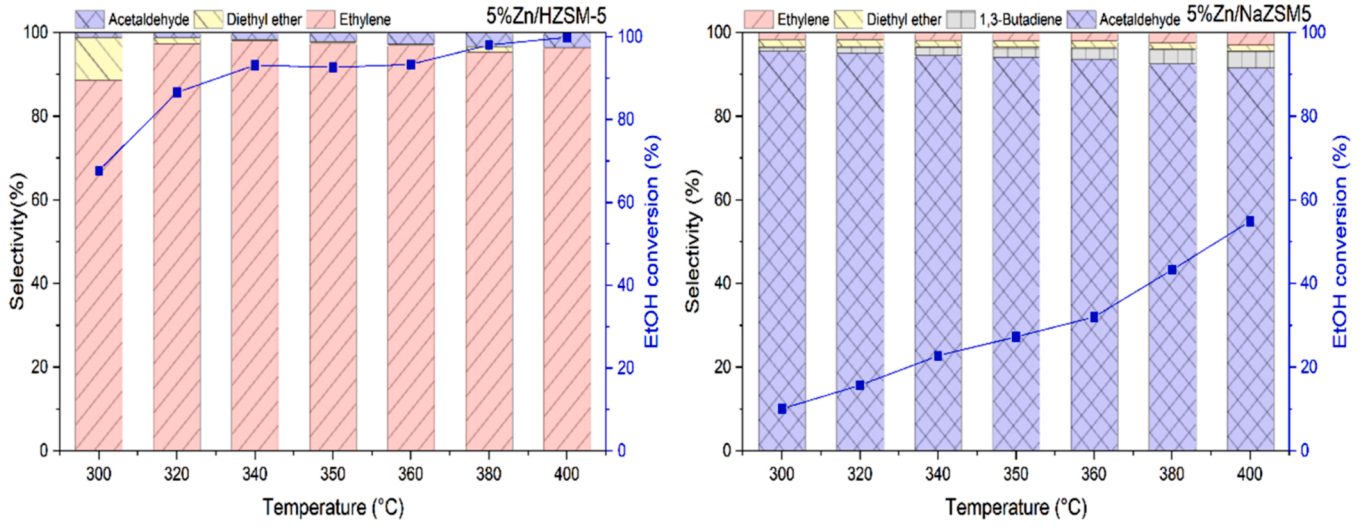

Fig. 6. The conversion and selectivity for the catalytic dehydrogenation of ethanol over 5% Zn/HZSM-5% and 5% Zn/NaZSM-5 catalysts.

CRediT authorship contribution statement

Kai Gao: Conceptualization, Methodology, Validation, Formal analysis, Investigation, Writing–Original Draft, Writing – Review & Editing, Visualization. **Jerrik Mielby:** Conceptualization, Methodology, Formal analysis, Investigation, Resources, Writing–Original Draft, Writing – Review & Editing, Visualization, Supervision. **Søren Kegnæs:** Conceptualization, Methodology, Formal analysis, Investigation, Resources, Writing–Original Draft, Writing – Review & Editing, Visualization, Supervision, Project administration, Funding acquisition.

Declaration of Competing Interest

The authors declare the following financial interests/personal relationships which may be considered as potential competing interests: Søren Kegnæs reports financial support was provided by Independent Research Fund Denmark. Søren Kegnæs reports financial support was provided by Villum Foundation. Søren Kegnæs reports financial support was provided by Haldor Topsøe A/S. Kai Gao reports financial support was provided by China Scholarship Council. Søren Kegnæs reports a relationship with China University of Petroleum Huadong that includes: speaking and lecture fees.: Søren Kegnæs reports financial upport was provided by Independent Research Fund Denmark. Søeren Kegnaes reports financial support was provided by Villum Foundation. Soeren Kegnaes reports financial support was provided by Haldor Topsoe AS. Kai Gao reports financial support was provided by China Scholarship Council. Soeren Kegnaes reports a relationship with China University of Petroleum Huadong that includes: speaking and lecture fees.

Acknowledgments

This work was supported by Haldor Topsøe A/S, Independent Research Fund Denmark (grant no. 6111-00237 and 0217-00146B), Villum fonden (Grant No. 13158) and the European Union's Horizon 2020 research and innovation programme under grant agreement No 872102. The authors gratefully acknowledge the Department of Chemistry, Technical University of Denmark (DTU) for the support of the project. Dr. Farnoosh Goodarzi and Mikkel Kock Larsen are also appreciated for their generous help with SEM images and fruitful discussions. Kai Gao would like to thank China Scholarship Council (CSC) for financial support.

Appendix A. Supporting information

Supplementary data associated with this article can be found in the online version at doi:10.1016/j.cattod.2022.06.023.

References

[1] R. Jira, Acetaldehyde from ethylene - a retrospective on the discovery of the wacker process, Angew. Chem. Int. Ed. 48 (2009) 9034–9037, https://doi.org/10.1002/anie.200903992.
[2] J.L. Wang, L.N. He, C.X. Miao, Y.N. Li, Ethylene carbonate as a unique solvent for palladium-catalyzed Wacker oxidation using oxygen as the sole oxidant, Green Chem. 11 (2009) 1317–1320, https://doi.org/10.1039/b913779n.
[3] C.H. Christensen, B. Jørgensen, J. Rass-Hansen, K. Egeblad, R. Madsen, S. K. Klitgaard, S.M. Hansen, M.R. Hansen, H.C. Andersen, A. Riisager, Formation of acetic acid by aqueous-phase oxidation of ethanol with air in the presence of a heterogeneous gold catalyst, Angew. Chem. Int. Ed. 118 (2006) 4764–4767, https://doi.org/10.1002/ange.200601180.
[4] Y.Y. Gorbanev, S. Kegnæs, C.W. Hanning, T.W. Hansen, A. Riisager, Acetic acid formation by selective aerobic oxidation of aqueous ethanol over heterogeneous ruthenium catalysts, ACS Catal. 2 (2012) 604–612, https://doi.org/10.1021/cs200554h.
[5] A.B. Laursen, Y.Y. Gorbanev, F. Cavalca, P. Malacrida, A. Kleiman-Schwarsctein, S. Kegnæs, A. Riisager, I. Chorkendorff, S. Dahl, Highly dispersed supported ruthenium oxide as an aerobic catalyst for acetic acid synthesis, Appl. Catal. A Gen. 433–434 (2012) 243–250, https://doi.org/10.1016/j.apcata.2012.05.025.
[6] Y. Gucbilmez, T. Dogu, S. Balci, Ethylene and acetaldehyde production by selective oxidation of ethanol using mesoporous V-MCM-41 catalysts, Ind. Eng. Chem. Res. 45 (2006) 3496–3502, https://doi.org/10.1021/ie050952j.
[7] J. Xu, X.C. Xu, X.J. Yang, Y.F. Han, Silver/hydroxyapatite foam as a highly selective catalyst for acetaldehyde production via ethanol oxidation, Catal. Today 276 (2016) 19–27, https://doi.org/10.1016/j.cattod.2016.03.001.
[8] P. Liu, E.J.M. Hensen, Highly efficient and robust Au/MgCuCr2O4 catalyst for gas-phase oxidation of ethanol to acetaldehyde, J. Am. Chem. Soc. 135 (2013) 14032–14035, https://doi.org/10.1021/ja406820f.
[9] R. Pulikkal Thumbayil, D.B. Christensen, J. Mielby, S. Kegnæs, Dehydrogenation of bioethanol using Cu nanoparticles supported on N-doped ordered mesoporous carbon, ChemCatChem 12 (2020) 5644–5655, https://doi.org/10.1002/cctc.202000883.
[10] W.H. Cassinelli, L. Martins, A.R. Passos, S.H. Pulcinelli, A. Rochet, V. Briois, C. V. Santilli, Correlation between structural and catalytic properties of copper supported on porous alumina for the ethanol dehydrogenation reaction, ChemCatChem 7 (2015) 1668–1677, https://doi.org/10.1002/cctc.201500112.
[11] G. Garbarino, P. Riani, M. Villa García, E. Finocchio, V. Sanchez Escribano, G. Busca, A study of ethanol dehydrogenation to acetaldehyde over copper/zinc aluminate catalysts, Catal. Today 354 (2020) 167–175, https://doi.org/10.1016/j.cattod.2019.01.002.
[12] D. Yu, W. Dai, G. Wu, N. Guan, L. Li, Stabilizing copper species using zeolite for ethanol catalytic dehydrogenation to acetaldehyde, Chin. J. Catal. 40 (2019) 1375–1384, https://doi.org/10.1016/S1872-2067(19)63378-4.
[13] S. Hanukovich, A. Dang, P. Christopher, Influence of metal oxide support acid sites on Cu-catalyzed nonoxidative dehydrogenation of ethanol to acetaldehyde, ACS Catal. 9 (2019) 3537–3550, https://doi.org/10.1021/acscatal.8b05075.
[14] M. Ohira, H. Liu, D. He, Y. Hirata, M. Sano, T. Suzuki, T. Miyake, Catalytic performance and reaction pathways of Cu/SiO2 and ZnO/SiO2 for dehydrogenation of ethanol to acetaldehyde, J. Jpn. Pet. Inst. 61 (2018) 205–212, https://doi.org/10.1627/jpi.61.205.
[15] H. Zhang, H.R. Tan, S. Jaenicke, G.K. Chuah, Highly efficient and robust Cu catalyst for non-oxidative dehydrogenation of ethanol to acetaldehyde and hydrogen, J. Catal. 389 (2020) 19–28, https://doi.org/10.1016/j.jcat.2020.05.018.
[16] H.T. Abdulrazzaq, A. Rahmani Chokanlu, B.G. Frederick, T.J. Schwartz, Reaction kinetics analysis of ethanol dehydrogenation catalyzed by MgO-SiO2, ACS Catal. 10 (2020) 6318–6331, https://doi.org/10.1021/acscatal.0c00811.
[17] A. Neramittagapong, W. Attaphaiboon, S. Neramittagapong, Acetaldehyde production from ethanol over Ni-based catalysts, Chiang Mai J. Sci. 35 (2008) 171–177.
[18] J. Shan, N. Janvelyan, H. Li, J. Liu, T.M. Egle, J. Ye, M.M. Biener, J. Biener, C. M. Friend, M. Flytzani-Stephanopoulos, Selective non-oxidative dehydrogenation of ethanol to acetaldehyde and hydrogen on highly dilute NiCu alloys, Appl. Catal. B Environ. 205 (2017) 541–550, https://doi.org/10.1016/j.apcatb.2016.12.045.
[19] S. Luo, H. Song, D. Philo, M. Oshikiri, T. Kako, J. Ye, Solar-driven production of hydrogen and acetaldehyde from ethanol on Ni-Cu bimetallic catalysts with solar-to-fuels conversion efficiency up to 3.8%, Appl. Catal. B Environ. 272 (2020), 118965 https://doi.org/10.1016/j.apcatb.2020.118965.
[20] G. Giannakakis, A. Trimpalis, J. Shan, Z. Qi, S. Cao, J. Liu, J. Ye, J. Biener, M. Flytzani-Stephanopoulos, NiAu single atom alloys for the non-oxidative dehydrogenation of ethanol to acetaldehyde and hydrogen, Top. Catal. 61 (2018) 475–486, https://doi.org/10.1007/s11244-017-0883-0.
[21] G. Garbarino, P. Riani, M. Villa García, E. Finocchio, V. Sánchez Escribano, G. Busca, A study of ethanol conversion over zinc aluminate catalyst, Reac. Kinet. Mech. Cat. 124 (2018) 503–522, https://doi.org/10.1007/s11144-018-1395-z.
[22] E. Seker, The catalytic reforming of bio-ethanol over SiO2 supported ZnO catalysts: the role of ZnO loading and the steam reforming of acetaldehyde, Int. J. Hydrog. Energy 33 (2008) 2044–2052, https://doi.org/10.1016/j.ijhydene.2008.02.033.
[23] M.J. Chung, S.H. Han, K.Y. Park, S.K. Ihm, Differing characteristics of Cu and ZnO in dehydrogenation of ethanol: a deuterium exchange study, J. Mol. Catal. 79 (1993) 335–345, https://doi.org/10.1016/0304-5102(93)85113-8.
[24] S.J. Raynes, R.A. Taylor, Zinc oxide-modified mordenite as an effective catalyst for the dehydrogenation of (bio)ethanol to acetaldehyde, Sustain. Energy Fuels (2021), https://doi.org/10.1039/d1se00091h.
[25] J. Mielby, J.O. Abildstrøm, F. Wang, T. Kasama, C. Weidenthaler, S. Kegnæs, Oxidation of bioethanol using zeolite-encapsulated gold nanoparticles, Angew. Chem. Int. Ed. (2014) 12721–12724, https://doi.org/10.1002/ange.201406354.
[26] Y. Guan, E.J.M. Hensen, Ethanol dehydrogenation by gold catalysts: the effect of the gold particle size and the presence of oxygen, Appl. Catal. A Gen. 361 (2009) 49–56, https://doi.org/10.1016/j.apcata.2009.03.033.
[27] T. Maihom, M. Probst, J. Limtrakul, Density functional theory study of the dehydrogenation of ethanol to acetaldehyde over the Au-exchanged ZSM-5 zeolite: effect of surface oxygen, J. Phys. Chem. C 118 (2014) 18564–18572, https://doi.org/10.1021/jp505002u.
[28] C. Wang, G. Garbarino, L.F. Allard, F. Wilson, G. Busca, M. Flytzani-Stephanopoulos, Low-temperature dehydrogenation of ethanol on atomically dispersed gold supported on ZnZrOx, ACS Catal. 6 (2016) 210–218, https://doi.org/10.1021/acscatal.5b01593.
[29] M.V. Twigg, M.S. Spencer, Deactivation of copper metal catalysts for methanol decomposition, methanol steam reforming and methanol synthesis, Top. Catal. 22 (2003) 191–203, https://doi.org/10.1023/A:1023567718303.
[30] F.W. Chang, W.Y. Kuo, K.C. Lee, Dehydrogenation of ethanol over copper catalysts on rice husk ash prepared by incipient wetness impregnation, Appl. Catal. A Gen. 246 (2003) 253–264, https://doi.org/10.1016/S0926-860X(03)00050-4.
[31] M. Ouyang, S. Cao, S. Yang, M. Li, M. Flytzani-Stephanopoulos, Atomically dispersed Pd supported on zinc oxide for selective nonoxidative ethanol dehydrogenation, Ind. Eng. Chem. Res. 59 (2020) 2648–2656, https://doi.org/10.1021/acs.iecr.9b05202.

[32] J. Sun, K. Zhu, F. Gao, C. Wang, J. Liu, C.H.F. Peden, Y. Wang, Direct conversion of bio-ethanol to isobutene on nanosized ZnxZryOz mixed oxides with balanced acid-base sites, J. Am. Chem. Soc. 133 (2011) 11096–11099.
[33] F. Goodarzi, L. Kang, F.R. Wang, F. Joensen, S. Kegnæs, J. Mielby, Methanation of carbon dioxide over zeolite-encapsulated nickel nanoparticles, ChemCatChem 10 (2018) 1566–1570, https://doi.org/10.1002/cctc.201701946.
[34] K.H. Rasmussen, F. Goodarzi, D.B. Christensen, J. Mielby, S. Kegnæs, Stabilization of metal nanoparticle catalysts via encapsulation in mesoporous zeolites by steam-assisted recrystallization, ACS Appl. Nano Mater. 2 (2019) 8083–8091, https://doi.org/10.1021/acsanm.9b02205.
[35] US5208201 A, The British Petroleum Company P.L.C., (1993) 1–8.
[36] M. Hamidzadeh, S. Komeili, M. Saeidi, Seed-induced synthesis of ZSM-5 aggregates using the Silicate-1 as a seed: characterization and effect of the Silicate-1 composition, Microporous Mesoporous Mater. 268 (2018) 153–161, https://doi.org/10.1016/j.micromeso.2018.04.016.
[37] X. Su, W. Zan, X. Bai, G. Wang, W. Wu, Synthesis of microscale and nanoscale ZSM-5 zeolites: effect of particle size and acidity of Zn modified ZSM-5 zeolites on aromatization performance, Catal. Sci. Technol. 7 (2017) 1943–1952, https://doi.org/10.1039/c7cy00435d.
[38] S. Cheng, L. Wei, J. Julson, K. Muthukumarappan, P.R. Kharel, Y. Cao, E. Boakye, D. Raynie, Z. Gu, Hydrodeoxygenation upgrading of pine sawdust bio-oil using zinc metal with zero valency, J. Taiwan Inst. Chem. Eng. 74 (2017) 146–153, https://doi.org/10.1016/j.jtice.2017.02.011.
[39] X. Niu, J. Gao, Q. Miao, M. Dong, G. Wang, W. Fan, Z. Qin, J. Wang, Influence of preparation method on the performance of Zn-containing HZSM-5 catalysts in methanol-to-aromatics, Microporous Mesoporous Mater. 197 (2014) 252–261, https://doi.org/10.1016/j.micromeso.2014.06.027.
[40] K. Egeblad, M. Kustova, S.K. Klitgaard, K. Zhu, C.H. Christensen, Mesoporous zeolite and zeotype single crystals synthesized in fluoride media, Microporous Mesoporous Mater. 101 (2007) 214–223, https://doi.org/10.1016/j.micromeso.2006.11.001.